Reconciliation of continuum and atomistic models for the ductile versus brittle response of iron

Glenn E Beltz¹ and Anna Machová²

- ¹ Department of Mechanical Engineering, University of California, Santa Barbara, CA 93106-5070, USA
- 2 Institute of Thermomechanics, Academy of Sciences of the Czech Republic, Dolejskova 5, 18200 Prague 8, Czech Republic

Received 31 March 2006, in final form 13 October 2006 Published 4 January 2007 Online at stacks.iop.org/MSMSE/15/65

Abstract

We present a detailed analysis of the ductile versus brittle response of bcc iron containing a sharp crack and show that a continuum model based on the Peierls-Nabarro model for dislocation formation is consistent with our atomistic results. Specifically, we compare continuum predictions for dislocation emission from a crack tip loaded in mode I under plane strain, tensile conditions with atomistic results for a $(\bar{1} \ 10)[1 \ 10]$ crack emitting full edge dislocations in the $\langle 1 \ 1 \ 1 \rangle$ $\{112\}$ slip system. The simulations are based on an N-body potential of the Finnis-Sinclair type for iron at 0 K, and the continuum dislocation model incorporates recent improvements that account for tension-shear coupling on a prescribed slip plane, as well as the T-stress, in an anisotropic solid. We show that the critical load for dislocation nucleation is influenced by the T-stress (modulated by the level of external stress applied parallel to the crack plane in a biaxially-loaded plate), which possesses a critical value associated with a change of mechanism between dislocation emission and crack extension. The results are consistent with recent preliminary analyses that address the effect of crack size and the role of the T-stress in the ductile versus brittle response of crystals.

1. Introduction

In the study of the mechanical response of crystals, an in-depth comparison of continuum and atomistic results is essential, since two independent approaches can validate less-proven methodologies and build overall confidence regarding the phenomena under investigation. However, the analysis of discrepancies between these approaches (e.g. [1–4]) is not trivial since, unlike continuum elastic models, atomistic simulations (i) do not involve stress singularities that are associated with crack tips and dislocation cores and (ii) may be influenced by border conditions associated with a finite domain.

Recent results on ductile versus brittle response indicate that existing contradictions between atomistic results, e.g. [3], and the continuum prediction by Rice [5] based on the Peierls–Nabarro model can be overcome when normal relaxation [6] between the slip planes

and the T-stress acting along the crack plane [7] are included in the continuum model. Until now, these effects have been treated separately. In this paper, a new continuum approach that simultaneously includes *both* normal relaxation and the T-stress effect is described. We present here in detail the energy and stress analysis of dislocation emission under uniaxial loading in mode I in a single crystal of α -iron. The simulations have been carried out for larger samples than previously considered and have been performed for various amounts of load applied both perpendicular and parallel to the crack face. The continuum model developed for this paper is used for an anisotropic solid, in order to make the comparison with the atomistic results as self-consistent as possible.

The details of the stress state around a crack tip in an elastic solid are often characterized by a single parameter, the stress intensity factor K that expresses the strength of the singularity as the crack tip is approached. This parameter is extremely useful for quantifying when a crack might begin to propagate or when it may emit a dislocation (or other shear-like feature) and subsequently blunt. It has long been recognized that a nonsingular contribution to the stress field (that is, a term that remains finite as the crack tip is approached, also known as the 'T-stress') may have some bearing on the stability of a propagating crack. However, the effects of including the T-stress in models for dislocation nucleation have largely been ignored until recently. Beltz and coworkers [8] incorporated this term into the Rice model [5] for dislocation nucleation at a crack tip in an isotropic medium. It was found that in addition to the unstable stacking energy γ_{us} (introduced in [5] in connection with block-like shear (BLS) displacement of a crystal), the T-stress is also important and it has a profound impact on the brittle-ductile behaviour of short cracks. This paper demonstrates the importance of the T-stress in atomistic simulations. Moreover, we consider the influence of normal relaxation of slip planes (i.e. the tension-shear coupling effect, as described by Sun et al [9]). Both effects can decrease the applied load needed for dislocation emission, and hence it is incumbent to properly account for these effects when attempting to reconcile atomistic simulations (e.g. [3,4]) with continuumbased predictions

Another important consideration is the relative orientation of the crack plane and available slip systems. Molecular dynamic (MD) simulations in bcc iron using the *N*-body potential [10, 11] have shown that for the crack orientation $(0\,0\,1)[1\,1\,0]$ (crack plane/crack front direction), the generation of unstable stacking faults and twinning at the crack tip are preferred on the $\langle 1\,1\,1 \rangle$ {112} slip systems; while for the crack orientation $(\bar{1}\,1\,0)[1\,1\,0]$, emission of complete edge dislocations is observed on the same type of slip systems [12], using the same potential [11] as in our work. The stress and energy analysis presented here show that this can be explained by the fact that the active shear systems $\langle 1\,1\,1 \rangle \{1\,1\,2\}$ are oriented in the 'easy,' or twinning, direction for the crack $(0\,0\,1)[1\,1\,0]$ and in the 'hard,' anti-twinning direction for the crack $(\bar{1}\,1\,0)[1\,1\,0]$.

Our continuum and atomistic models use the concept of the so-called interplanar stress [5], since it is able to adequately describe the stress gradient arising at an interface when straining is inhomogeneous in the range of the interatomic interactions [13–15].

2. Continuum predictions in anisotropic materials

2.1. Strain and stress fields

For a homogeneous anisotropic material under plane strain conditions ($\varepsilon_{zz} = \varepsilon_{zy} = \varepsilon_{zx} = 0$), the strain–stress relations may be written [16] by means of the symmetric compliance constants A_{ij} that can be determined from the 'unconstrained' compliances S_{ij} through the relation $A_{ij} = S_{ij} - S_3 S_{j3} / S_{33}$. Here we associate the cartesian axes (x, y, z) with crystallographic

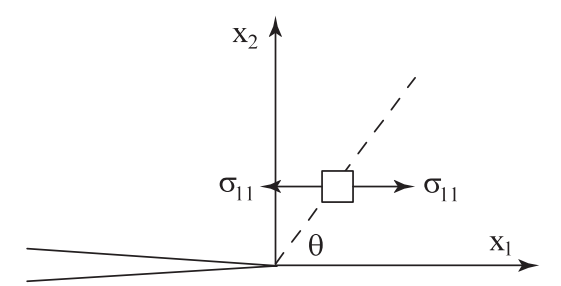


Figure 1. The crack and slip system inclined at angle θ . For convenience, the notations (x_1, x_2, x_3) and (x, y, z) are interchangeably used in the text to refer to a cartesian coordinate system based at the crack tip.

Table 1. Continuum predictions for dislocation nucleation threshold for various biaxiality ratios α .

α	0.0	0.1	0.2	0.3	0.4	0.5	0.6	0.7	0.8	0.9	1.0
$G_{\rm disl}/\gamma_{\rm us}$ isotropic shear only	4.27	4.34	4.61	4.79	4.98	5.19	5.41	5.64	5.88	6.14	6.42
$G_{\rm disl}/\gamma_{\rm us}$ anisotropic shear only	4.09	4.27	4.46	4.66	4.88	5.11	5.36	5.62	5.90	6.20	6.52
$G_{\rm disl}/\gamma_{\rm us}$ anisotropic t/s coupling	2.70	2.82	2.94	3.08	3.23	3.39	3.58	3.78	4.01	4.27	4.59

directions [0 0 1], [1 1 0] and [1 1 0], respectively. Due to the symmetry of this crystal orientation, the constants A_{16} and A_{26} vanish. The remaining constants (in units 10^{-11} m² N⁻¹) are $A_{11} = 0.5698$, $A_{12} = -0.2664$, $A_{22} = 0.4470$ and $A_{66} = 0.8621$. These values have been derived for our crystal orientation from the basic elastic constants C_{11} , C_{12} and C_{44} for the N-body potential from [11]³.

In cracked anisotropic bodies (see figure 1), the stress field depends not only on the nature of the applied loading (as in the isotropic case) but also on the elastic compliances through complex variables μ_1 and μ_2 , which in our case are $\mu_1 = 0.5462 + i0.7664$, $\mu_2 = -0.5462 + i0.7664$.

The stress field around a narrow central crack of the length 2a, embedded in a large crystal and loaded in tension mode I with an applied stress σ_A acting at the borders in the y-direction, has been given by Savin [17]. For the angle $\theta = 0^{\circ}$, the stress components σ_{xx} and σ_{yy} are given by

$$\sigma_{xx} = -\frac{\text{Re}(\mu_1 \mu_2) \sigma_A x}{\sqrt{x^2 - a^2}} + T, \qquad \sigma_{yy} = \frac{\sigma_A x}{\sqrt{(x^2 - a^2)}},$$
 (1)

where x = r + a, and r is the distance from the crack tip. The constant term $T = \text{Re}(\mu_1 \ \mu_2)\sigma_A$ represents the so called T-stress, which degenerates to $T = -\sigma_A$ in the isotropic case. In the limit $x \to \infty$, we obtain $\sigma_{yy} \to \sigma_A$ and $\sigma_{xx} \to 0$.

If the stress component σ_{yy} is written as an expansion about x = a, i.e.

$$\sigma_{yy} = \frac{\sigma_{A}}{\sqrt{x - a}} \left[\frac{x}{(x + a)^{1/2}} \right] = \frac{\sigma_{A}}{\sqrt{x - a}} \left[\sqrt{\frac{a}{2}} + \frac{3}{4\sqrt{2a}} (x - a) + \frac{5}{32a\sqrt{2a}} (x - a)^{2} + \cdots \right]$$
(2)

(and performing a similar exercise for σ_{xx}), it is evident that an asymptotic stress field for the angle $\theta=0^\circ$ can be re-expressed in terms of the stress intensity factor $K_{\rm I}=\sigma_{\rm A}\,(\pi\,a)^{1/2}$ and the T-stress as

$$\sigma_{xx} = -\frac{\operatorname{Re}(\mu_1 \mu_2) K_{\mathrm{I}}}{\sqrt{2\pi r}} + T, \qquad \sigma_{yy} = \frac{K_{\mathrm{I}}}{\sqrt{2\pi r}}.$$
 (3)

³ Note that a printing error exists in [11]. The correct units for the parameters a_i and A_i in table 1 contained therein are eV/a_0^3 and eV^2/a_0^3 , respectively.

If an additional external load $\sigma_B = \alpha \sigma_A$ is superposed in the x-direction, then the stress intensity factor is unchanged but T changes as described by Stroh [18]:

$$T = \sigma_{\mathcal{A}} \left[\operatorname{Re}(\mu_1 \mu_2) + \alpha \right]. \tag{4}$$

The case $\alpha=0$ corresponds to pure mode I under *uniaxial*, far-field tension, while the case $\alpha=1$ corresponds to mode I induced by a *biaxial*, far-field loading $\sigma_B=\sigma_A$.

The energy release rate G is given by the relation $G = CK_1^2$, where C is an appropriate factor based on the constants A_{ij} [16]; in our case, C takes the value 3.868×10^{-12} m² N⁻¹. The anisotropic constant Re($\mu_1 \mu_2$) is -0.8857. A comparison of stress components from relations (3) and (4) with the stresses derived from the atomistic level will be given in section 4.2.

2.2. Ductile/brittle predictions

It is well known that the T-stress influences shear processes at crack tips [8, 19]. Moreover, an established model for the prediction of the ductile/brittle behaviour in an anisotropic continuum is at our disposal: the Peierls framework for dislocation formation at a crack, which assumes that the dislocation/crack system can be thought of as two anisotropic elastic semi-spaces separated by a common plane (the crack plane and slip plane) on which there is a discontinuous jump in the displacement field [5,9,20]. This model makes use of a periodic relationship between shear stress and slip displacements along the slip plane, with traction free surfaces along the crack plane. Prior to dislocation nucleation, a distribution of slip discontinuity develops along the slip plane that ultimately reaches a point of instability with increased applied load. Using this theory, a locus of threshold $K_{\rm I}$ and T values at which nucleation occurs may be determined.

We implement this model at two different levels of complexity: (i) we use only a simple relationship due to Frenkel [21] between shear stress τ and slip displacement Δ_x on the slip plane,

$$\tau(\Delta_x) = \frac{\mu b}{2\pi h} \sin\left(\frac{2\pi \Delta_x}{b}\right) = \frac{\pi \gamma_{\text{us}}}{b} \sin\left(\frac{2\pi \Delta_x}{b}\right),\tag{5}$$

where τ is the shear stress ($\sigma_{r\theta}$ using the coordinates implied in figure 1), h is the interplanar spacing, μ is the 'effective' shear modulus for shear along the slip plane of interest (and can be written in terms of the anisotropic elastic constants), b is the Burgers vector and γ_{us} is the unstable stacking energy (equal to $\mu b^2/2\pi^2 h$ in the Frenkel model) and (ii) we consider combined slip Δ_x and opening displacements Δ_y (normal relaxation) on the slip plane, which may be written as $\tau = \partial \phi/\partial \Delta_x$ and $\sigma = \partial \phi/\partial \Delta_y$, with the potential function proposed by Rice and coworkers [9] as

$$\phi(\Delta_x, \ \Delta_y) = 2\gamma_s \left(1 - \left(1 + \frac{\Delta_y}{L} \right) e^{-\Delta_y/L} + \sin^2\left(\frac{\pi \Delta_x}{b}\right) \left\{ q + \left(\frac{q-p}{1-p}\right) \frac{\Delta_y}{L} \right\} e^{-\Delta_y/L} \right), \tag{6}$$

where γ_s is the surface energy for the separating surfaces, L is the characteristic length of the decohesion process (i.e. tensile stress undergoes a maximum at $\Delta_y = L$ in the absence of any shear deformation) and p and q are dimensionless material constants that quantify the degree of tension–shear coupling. Specifically, q is defined as the ratio $\gamma_{us}/2\gamma_s$ (here, γ_{us} refers to an unrelaxed shear process, as elaborated upon by Sun et~al~[9]), and p is related to the dilatation undergone by the crystal when it shears to its unstable stacking position at zero normal stress.

In these slip plane constitutive equations, Δ_x is the relative atomic shear displacement between two atomic planes and Δ_y is the relative opening between the planes. As introduced by Rice [5], we use the continuum slip variable δ_x , thought of as Δ_x extrapolated to a cut

halfway between the slipping planes and given by $\delta_x = \Delta_x - \tau h/\mu$ (and similarly for δ_y versus Δ_y). From equilibrium considerations, the stress along the slip plane can be written as

$$\tau \left[\delta_{x}, \delta_{y} \right] = \frac{K_{1} S_{r\theta}(\theta)}{\sqrt{2\pi r}} - T \sin \theta \cos \theta - \int_{0}^{\infty} g_{11}(r, s, \theta) \frac{\partial \delta_{x}(s)}{\partial s} ds - \int_{0}^{\infty} g_{12}(r, s, \theta) \frac{\partial \delta_{y}(s)}{\partial s} ds,$$

$$(7a)$$

$$\sigma \left[\delta_{x}, \delta_{y} \right] = \frac{K_{1} S_{\theta\theta}(\theta)}{\sqrt{2\pi r}} + T \sin^{2} \theta - \int_{0}^{\infty} g_{21}(r, s, \theta) \frac{\partial \delta_{x}(s)}{\partial s} ds - \int_{0}^{\infty} g_{22}(r, s, \theta) \frac{\partial \delta_{y}(s)}{\partial s} ds.$$

$$(7b)$$

The first two terms on the right-hand side of each equation give the pre-existing stress along the slip plane due to the applied load on the crack geometry (comprising the most singular term, scaled by $K_{\rm I}$, as well as the constant term, proportional to T, and the angular dependences $S_{r\theta}$ and $S_{\theta\theta}$ for cracks in an anisotropic solid), and the third and fourth terms reflect the stress relaxation that occurs due to sliding along the cut. The kernel functions g_{ij} in the integral term represent the stresses at distance r along the slip plane in an anisotropic solid due to a dislocation positioned at s, while $(-\partial \delta_x/\partial s)$ ds and $(-\partial \delta_y/\partial s)$ ds represent infinitesimal Burgers vectors (we exploit the notion that the slip distribution can be discretized into an array of infinitesimal dislocations). We seek slip and opening distributions $\delta_x(r)$ and $\delta_y(r)$ such that, for all r > 0, τ and σ predicted by the formulation above (equations (7a) and (7b)), must equate to τ and σ provided by the atomic-based Frenkel relation. Using a numerical procedure outlined by Beltz [22] and Beltz and Rice [23], we carry this out for incremental increases in $K_{\rm I}$ and T, which are linearly related to each other through a relation $T = K[\alpha + \text{Re}(\mu_1 \ \mu_2)]/(\pi a)^{1/2}$, until an instability (i.e. dislocation nucleation) is attained.

We consider the slip systems $\langle 1\,1\,1 \rangle$ {112} inclined at angle $\theta = 54.7^{\circ}$ with respect to a crack ($\bar{1}\,1\,0$) [110] (plane/front) embedded in bcc iron with the basic elastic constants $C_{11} = 2.433$, $C_{12} = 1.450$ and $C_{44} = 1.160 \times 10^{11} \,\mathrm{N\,m^{-2}}$ [7, 11], which are consistent with the values of A_{ij} cited in section 2.1. The shear modulus for the $\langle 1\,1\,1 \rangle$ {112} slip system is $\mu = (C_{11} - C_{12} + C_{44})/3 = 0.714 \times 10^{11} \,\mathrm{N\,m^{-2}}$ [24]. According to a simple, approximate version of the Rice model [7] for an *isotropic* continuum, the applied energy $G_{\rm disl}$ needed for emission of edge dislocations is given in our case by the expression $G_{\rm disl}/\gamma_{\rm us} = 8/(1+\cos\theta) \sin^2\theta = 7.612$. However, the framework discussed in the preceding paragraphs allows us to do better.

Table 1 shows how significantly the situation is influenced by the T-stress and by the ratio of biaxial stress α according to the Beltz/Rice model, both in the isotropic ($\nu = 0.37$) and the anisotropic case, when normal relaxation is not considered ($\Delta y = 0$). The table has been calculated for the dimensionless quantities h/b = 0.4714 and a/b = 17.32 (crack length), relevant for MD simulations. Here $h = a_0 / \sqrt{6}$ is the interplanar distance between the $\{1 \ 1 \ 2\}$ planes, $b = a_0 \sqrt{3/2}$ is the Burgers vector and a_0 is the lattice parameter in bcc iron. The largest impact (almost 50%) on the threshold for dislocation emission occurs for $\alpha = 0$, where $T = -\sigma_{\rm A}$ in the isotropic case and $T = -0.8857\sigma_{\rm A}$ in the anisotropic case. The negative values of the T stress decrease the threshold for dislocation emission. When the biaxiality ratio α increases, dislocation generation becomes more difficult and the ductile-brittle transition may occur at a certain value of α according to this new continuum prediction. The last row in table 1 for $\Delta_y \neq 0$ illustrates that a further decrease in G_{disl} may be caused by the normal relaxation in the continuum model. In figure 2, the anisotropic values $G_{\text{disl}}/\gamma_{\text{us}}$ from table 1 for $\Delta_{\gamma} \neq 0$ are plotted together with the horizontal line $2\gamma_s/\gamma_{us}$, that should predict the ductile/brittle interface in our MD simulations, since $2\gamma_s$ represents the theoretical work of decohesion for the potential used in a perfect crystal of bcc iron of the same orientation as defined above.

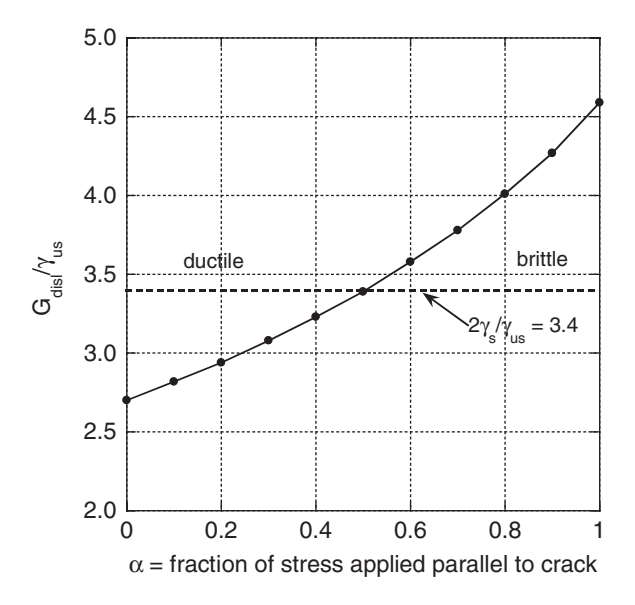


Figure 2. Threshold for dislocation nucleation as a function of biaxiality ratio α .

3. MD simulations

In all simulations described below, we utilize the *N*-body potential of the Finnis–Sinclair type for bcc iron that is discussed in previous studies [10, 11].

3.1. Perfect (uncracked) samples

In order to study lattice faulting generically, we first consider a perfect (uncracked) structure. Consider the bcc lattice projected onto a (1 1 0) plane. Each projected atom represents a chain of atoms in the perpendicular [1 1 0] direction. The crystal orientation is described in the previous section, and plane strain conditions are assumed. To simulate BLS in the 'hard,' anti-twinning direction, the upper part of the sample is fixed and the lower part is gradually displaced (step by step) in the $\langle 1 \ 1 \ 1 \rangle$ direction along a $\langle 1 \ 1 \ 2 \rangle$ plane in increments of 0.01b, where $b = a_0/2\langle 1 \ 1 \ 1 \rangle$ is the Burgers vector in bcc iron (see figure 3(a)). If we were interested in deformation twinning, the entire lower part of the crystal would be deformed as shown in figure 3(b) along the {112} planes in the (111) anti-twinning direction. Since there are more interplanar displacements and stresses associated with the atomistic analysis than what is allowed for in the continuum modelling of the previous section, we adopt a slightly different notation (U for displacements and R for stresses) in the context of the simulations to avoid confusion. Figure 3(c) illustrates that to reach the final mirror positions in the anti-twinning direction, the relative shear displacements below the plane 0 must be $U_{10} = U_{21} = U_{32} = \cdots = 2b/3$ (while in the easy twinning direction it is only b/3). In our notation for relative shear displacements, $U_{ij} \equiv U_i - U_j$, etc. For interplanar dimensionless stresses, $R_{ij}^* \equiv R_{ij} \times 1.303 \times 10^{-10} \, \text{Pa}$. The work done by the shear stresses is

$$W_{10} = \int R_{10} dU_{10}, \qquad W_{21} = \int R_{21} dU_{21}$$
 (8)

in the slip systems $\langle 1 \ 1 \ 1 \rangle \{ 1 \ 1 \ 2 \}$.

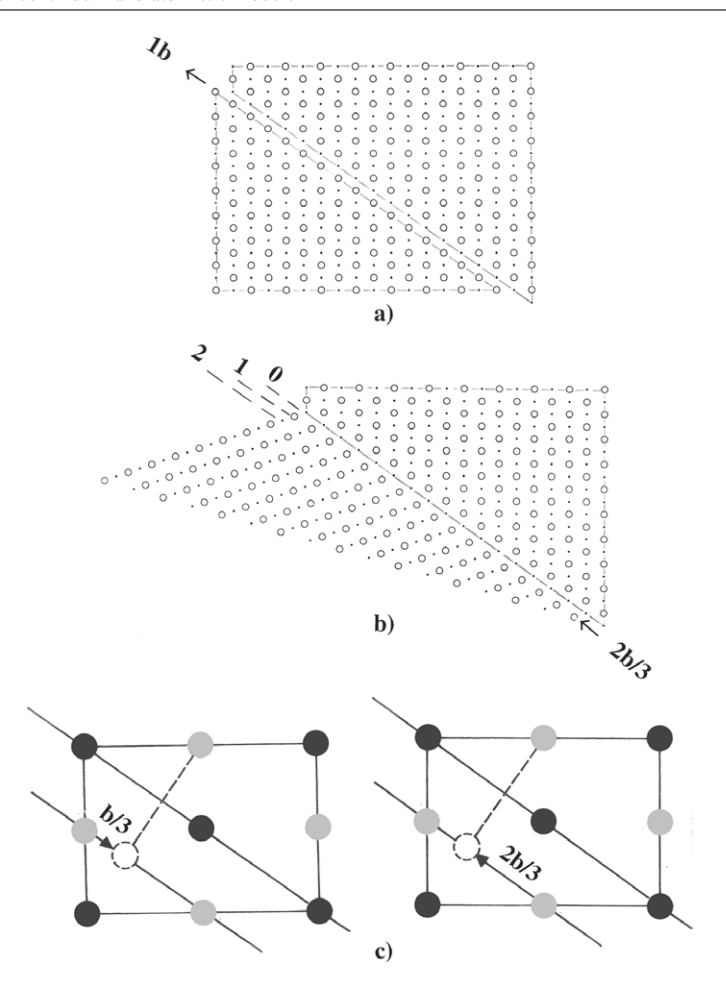


Figure 3. Schematics of (a) block-like shear (BLS); (b) deformation twinning; (c) the twinning (easy) and anti-twinning (hard) direction.

In earlier work, it has been shown that the resistance to BLS in the twinning and antitwinning directions are identical; i.e. $\gamma_{\rm us} = W_{10} = 1.14\,\rm J\,m^2$, and $\tau_{\rm c}^* = R_{10}^* = 2.13$ [10]. A different situation occurs during multi-plane shear in the anti-twinning direction (see figures 4 and 5), in which $W_{10} = 1.195\,\rm J\,m^{-2}$, $W_{21} = 1.433\,\rm J\,m^{-2}$, $W_{10} = 2.89$ and $W_{21} = 3.64$. That is, the lattice resistance to shear in the anti-twinning direction is substantially larger than that for the twinning direction. For a crack with slip systems oriented in the anti-twinning direction, dislocation emission (not twinning) is expected (see figure 6). The results are in agreement with previous theoretical work based on symmetry considerations [25] and with atomistic simulations using different potentials for bcc iron than those used in this study [26].

The influence of normal relaxation of the $\{1\,1\,2\}$ slip planes during BLS has also been examined in uncracked samples. To illustrate this effect, we use a value $o/h_{112} = +0.0625$ observed in an earlier MD study of dislocation emission in iron [7]. Here, o denotes the opening and h_{112} the interplanar spacing of $\{1\,1\,2\}$ planes. Figures 7 and 8 show how the separation of $\{1\,1\,2\}$ planes decreases the lattice resistance in comparison with pure BLS. The unstable stacking energy γ_{us} is smaller by approximately 7%, while the critical shear stress

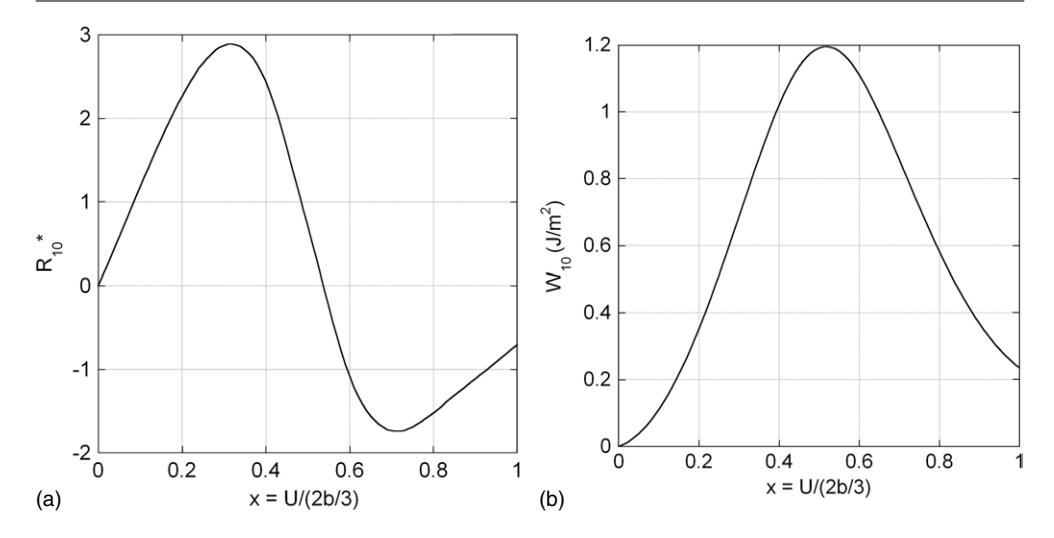


Figure 4. Dimensionless interplanar shear stress R_{10}^* and energy balance for interior atoms lying on plane 1 below the interface 0 during deformation twinning in the hard anti-twinning direction in uncracked samples.

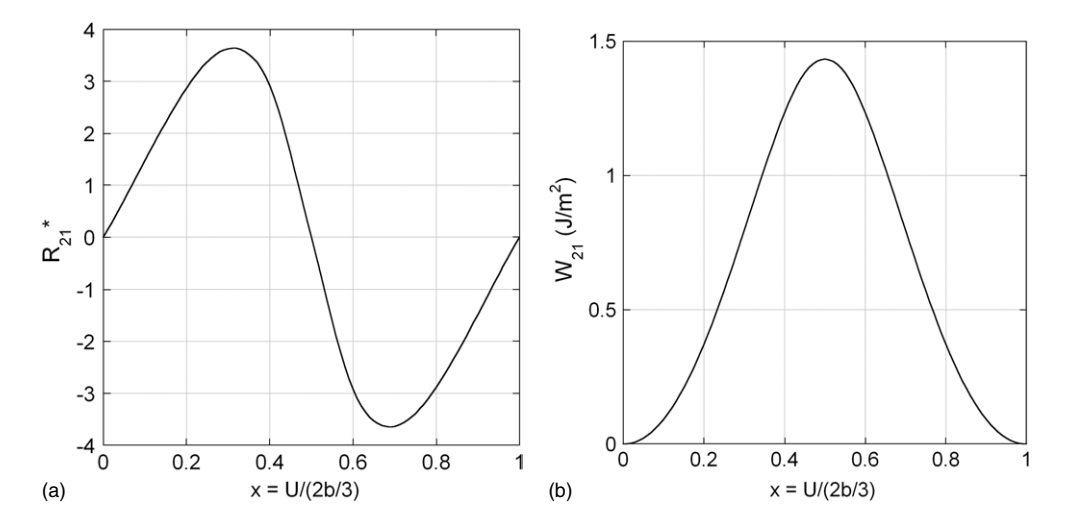


Figure 5. Dimensionless interplanar shear stress R_{21}^* and energy balance during the deformation anti-twinning for interior atoms lying on plane 2 below the interface 0.

 τ_c is smaller by approximately 10%. These observed behaviours are consistent with earlier simulations, and analytic modelling, carried out by Sun *et al* [9].

3.2. Cracked samples

We next consider a pre-existing atomically sharp central crack of the length $2\ell_0=2a$ embedded in a rectangular sample. The crack surfaces lie on $(\bar{1}\ 1\ 0)$ planes, the crack front is oriented along the z-direction and the potential crack extension is in the $x=[0\ 0\ 1]$ direction. The crack is loaded in mode I; i.e. the sample borders are loaded in the $\langle \bar{1}\ 1\ 0\rangle$ directions and we subsequently consider biaxial loading by adding load in the x-direction. Due to the symmetry

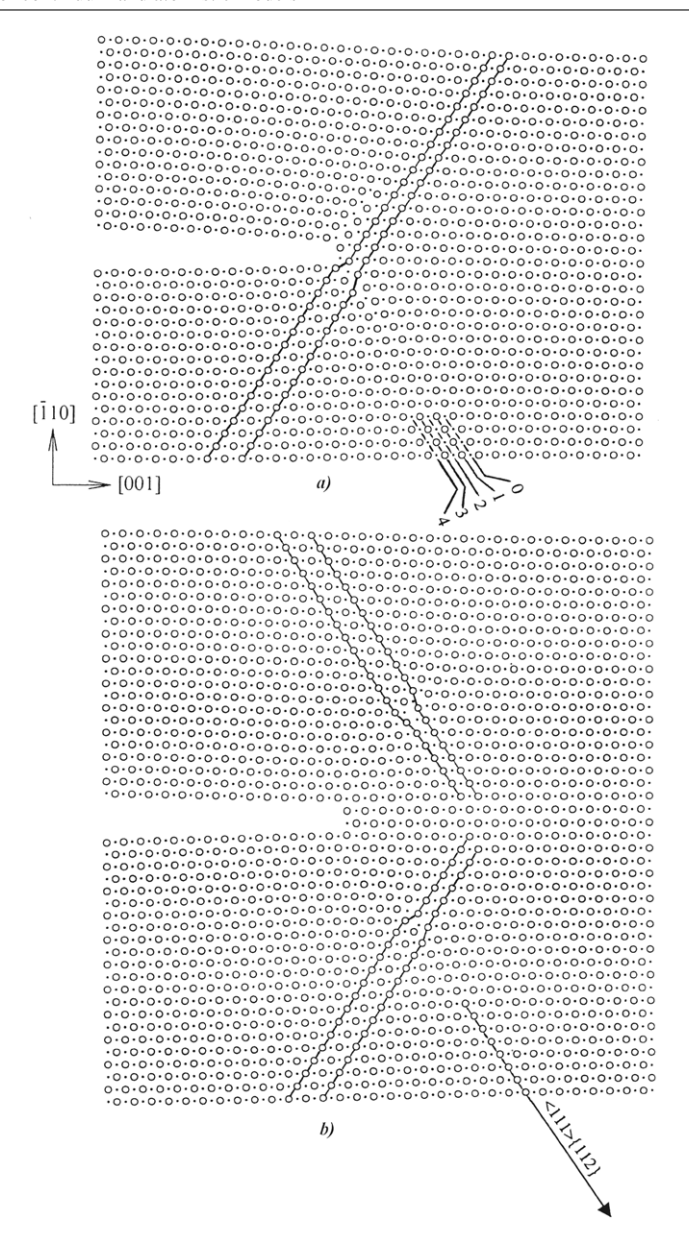


Figure 6. Generation (a) and emission (b) of complete edge dislocations from the crack ($\bar{1}$ 1 0)[1 1 0] loaded in mode I under the applied stress $\sigma_A = 6.82$ GPa (sample size 300 × 300).

of the problem, we only simulate one half of the sample in the x-direction. The external forces at individual surface atoms are distributed homogeneously in five border layers, as previously reported [10,11]. The sample consists of 300 planes both in the x and y directions for uniaxial loading and 432 planes in the y-direction for biaxial loading. To maintain symmetry, atoms lying at the left border of the sample (figure 6) are fixed in the x-direction, while other atoms are free to move in the x- and y-directions. The half crack length is $\ell_0 = 30 \ d_{001}$, where $d_{001} = a_0/2$ and $a_0 = 2.8665$ Å is the lattice parameter. Interatomic interactions across initial crack faces are not allowed.

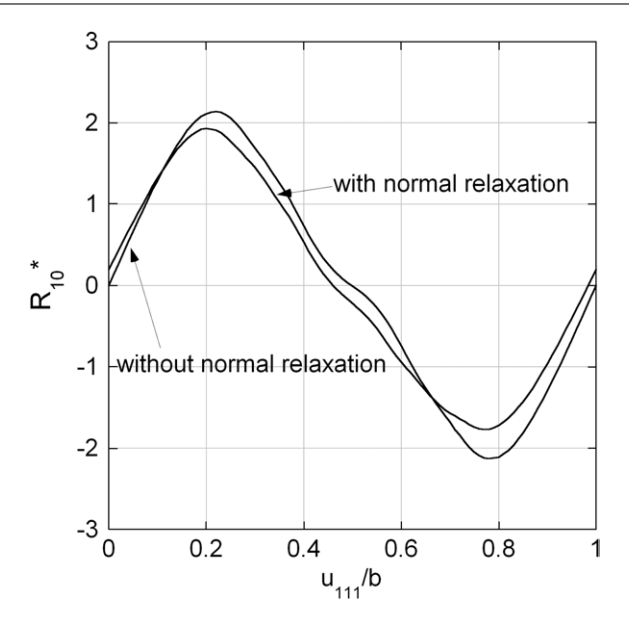


Figure 7. The decrease of the interplanar shear stress R_{10}^* in perfect samples when normal relaxation $o/h_{112} = 0.0625$ of the $\{1\,1\,2\}$ slip planes is included during BLS.

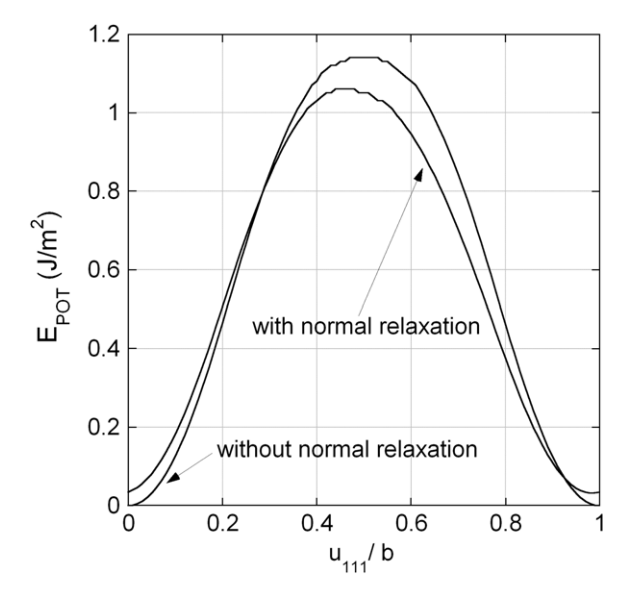


Figure 8. Change of the potential energy in perfect samples when normal relaxation $o/h_{112} = 0.0625$ of the {112} slip planes is introduced during BLS.

Prior to the external loading, the samples are relaxed to avoid the influence of surface relaxations on crack tip processes. The Newtonian equations of motion for individual atoms are solved by the central difference method using time integration steps of magnitude 10^{-14} s. Thermal atomic motion is not controlled in the system—that is, initial atomic velocities are set to zero and we do not use a 'thermostat' to control temperature, similar to earlier work by Mullins and Dokainish [1] or Machová and coworkers [10–12]. The global energy

balance $W_{\rm ext}(t) = E_{\rm pot}(t,0) + E_{\rm kin}(t)$ in the sample is monitored at each time step to ensure numerical stability in the system. Here, $W_{\rm ext}(t)$ denotes the work done by the external forces, $E_{\rm pot}(t,0) = E_{\rm pot}(t) - E_{\rm pot}(0)$ is the change of the total potential energy during loading and $E_{\rm kin}(t)$ is the total kinetic energy. We use a quasi-static loading, i.e. the total kinetic energy in the system is very low (similar to what is conveyed in figure 15 in [10]).

4. Discussion and comparison of results

4.1. Uniaxial loading

We first consider uniaxial tensile loading only. Here, the sample is loaded gradually to a level σ_A during 6000 time steps. When the prescribed stress level is reached, the applied stress is held constant. Dislocation emission is observed below the Griffith level $\sigma_G = K_G/\sqrt{\pi l_0}$, where K_G is the critical stress intensity factor given by the relation $2\gamma_s = CK_G^2$. Here γ_s is the surface energy and C is the appropriate anisotropic constant discussed in section 2.1. We note that the sample dimensions are sufficiently large compared with the crack size such that boundary correction procedures are not necessary [27].

Dislocation emission is not observed in the MD simulations at a constant level of applied stress $\sigma_A = 6.48$ GPa. At a slightly higher level, $\sigma_A = 6.82$ GPa, dislocation emission is observed with a certain delay (see figure 6). At an even higher level, $\sigma_A = 7.16$ GPa, dislocation emission occurs shortly after the constant stress level is attained. We define the point of dislocation emission as when the relative shear displacements ahead of the crack tip on the slip systems $\langle 1\,1\,1\rangle \{1\,1\,2\}$ exceed the value b. Figure 6 illustrates that a pair of edge dislocations have been emitted from the crack tip on the $\langle 1\,1\,1\rangle \{1\,1\,2\}$ slip systems. We note that the dislocations move away from the crack tip with a velocity smaller than the velocity of the shear waves in the slip system $\langle 1\,1\,1\rangle \{1\,1\,2\}$, in agreement with continuum expectations [12].

We performed a detailed energetic and stress analysis for a few key locations on the $\langle 1 \ 1 \ 1 \rangle \{1 \ 1 \ 2\}$ slip system. Specifically, we considered atoms on plane 1 (see figure 6) below the crack tip lying at distance b (crack tip atom) and 3b (interior atom) from the crack face. In addition to the time evolution of the relative shear displacements U_{10} , U_{21} , U_{32} and U_{43} , we also calculated the interplanar shear stress R_{10} at these two locations. From the histories of U_{10} and R_{10} we obtained a shear-displacement curve (R_{10} versus U_{10}) during dislocation emission (see figure 9). This curve differs somewhat from the ideal BLS results (figure 7) discussed earlier. The secondary maximum in the curve in figure 9 for the cracked sample coincides with a transient shear displacement of farther slip planes 2, 3, 4 near the critical point b/2. The shear stress R_{10} in figure 9 reaches its first zero point later than the corresponding BLS result, since there is a permanent nominal shear strain near the loaded crack, even after dislocation emission. The dependence R_{10} versus U_{10} enables one to calculate the work $W_{10} = \sum R_{10}(t_n) \Delta U_{10}(t_n)$ done by the shear stress during dislocation emission up to the point when R_{10} vanishes for the first time. This value W_{10} from the cracked sample should modestly correspond to the $\gamma_{\rm us}$ from the BLS result. At the crack tip atom we find that the value is $W_{10}(MD) = 1.06 \,\mathrm{J}\,\mathrm{m}^$ while at the interior atom it is $W_{10}(MD) = 1.245 \,\mathrm{J}\,\mathrm{m}^{-2}$. The average value from the MD simulation agrees well with γ_{us} from the BLS calculation. However, the peak stresses (at about $U_{10}/b \approx 0.2$, see figure 9) are significantly smaller than the expected value $\tau_c = 14.81 \, \text{GPa}$ following from the BLS (even including normal relaxation). This discrepancy can be explained by the influence of the T-stress.

The T-stress acts along the axis of potential crack extension, similar to the component S_{xx} from the MD simulation. According to the continuum plasticity theory [19], the influence

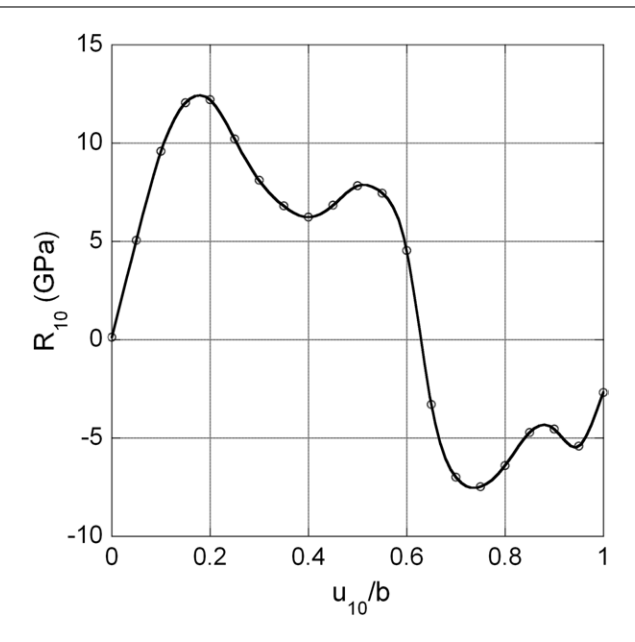


Figure 9. The shear–displacement curve at the interior atom in the $\langle 1\,1\,1 \rangle \{ 1\,1\,2 \}$ slip system, conceived according to figures 9 and 10 for $\sigma_A = 7.16$ GPa (sample size 300×300).

of the T-stress on the critical shear stress may be accounted for by the simple interchange $\tau_{\rm c} \to \tau_{\rm c} + T \sin \theta \cos \theta$, where θ is the angle of the inclined slip system with respect to the crack plane. For our crack and slip orientation (figure 6), the angle is $\theta \approx 55^{\circ}$ and $\sin \theta \cos \theta = 0.47$. According to a handbook of T values [28], for our geometry ($\ell_0/W = 0.1$, H/W = 0.707 and $\sigma_{\rm A} = 7.16$ GPa), T is about -6 GPa. It may decrease the value of the critical shear stress up to $\tau_{\rm c} = 11.98$ GPa, which is in good agreement with the peak stress shown in figure 9 ($R_{10} = 12.0$ –12.2 GPa) obtained from the MD simulations.

Dislocation emission in the simulations is observed at an applied stress intensity $K_{\rm IA} = 0.813 - 0.854 \, \text{MPa} \, \text{m}^{1/2}$. This is significantly lower than $K_{\rm disl} = 1.44 \, \text{MPa} \, \text{m}^{1/2}$ predicted by the Rice model when tension/shear coupling is included. We note that this is in qualitative agreement with the atomistic results in bcc iron obtained with a different potential for an equivalent crack orientation [3].

The influence of the T-stress in a simplified isotropic continuum model has been examined by Beltz and Fischer [8] as a function of crack size and slip plane inclination angle. Their model predicts the threshold is decreased by about 25% for our geometry. A more precise analysis of this effect in an anisotropic continuum according to table 1 for $\alpha=0$ gives better agreement with the MD results. Using the anisotropic constant $C=3.868\times10^{-12}$ m² N⁻¹ and the relaxed value of $\gamma_{\rm us}=1.06\,{\rm J\,m^{-2}}$, the lowest stress intensity factor needed for dislocation emission from the updated model including only the T-stress (no tension/shear coupling) is $K_{\rm disl}=1.059\,{\rm MPa\,m^{1/2}}$. Taking into account both the T-stress and the normal relaxation effects between slip planes ($G_{\rm disl}/\gamma_{\rm us}=2.70$ in table 1), we then obtain a predicted value $K_{\rm disl}=0.892\,{\rm MPa\,m^{1/2}}$, in good agreement with our MD results.

4.2. Biaxial loading

In our MD simulations of biaxially-loaded samples, the prescribed loading is linear up to $\sigma_A = 13.64$ GPa over 12 000 time steps. This is consistent with the loading rate used in the

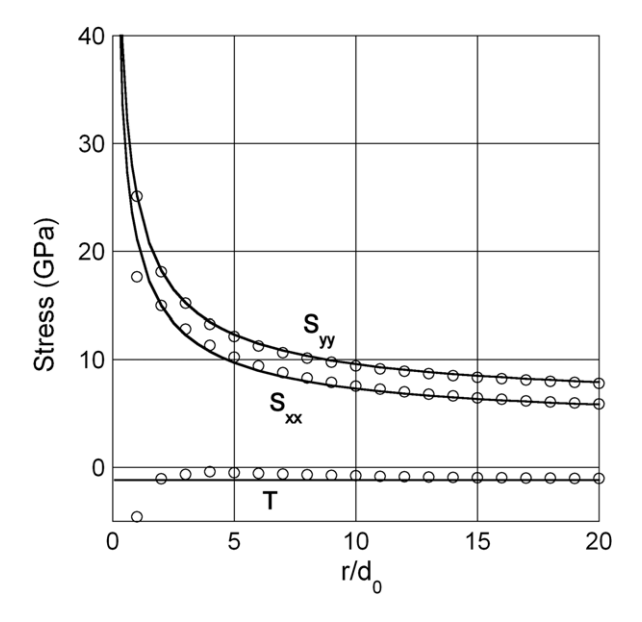


Figure 10. Comparison of the stress field in MD (o) at time step 6000 with continuum solution (——) for biaxiality ratio $\alpha=0.7$, $\sigma_{\rm A}=6.82$ GPa and angle $\theta=0^{\circ}$: normal stress component S_{yy} , lateral stress component S_{xx} and $T_{\rm a}$ stress (sample size 300×432).

previous section (prior to the constant level of the applied stress being attained). The sample consists of 300 planes in the x-direction and 432 planes in the y-direction. To ensure that loading waves in the x- and y-directions arrive from the borders to the crack tip at the same time, the sample size in the y-direction is increased for biaxial loading.

A comparison with the anisotropic elastostatic Savin–Stroh solution has been performed for a relatively low applied load (at time step 6000). In figure 10, we compare the interplanar [15] atomic stress (circles) ahead of the crack tip ($\theta=0^{\circ}$) with the Savin–Stroh solution (solid lines) for $\sigma_A=6.341$ GPa and for $\alpha=0.7$ (a regime in which no bond breakage and no dislocation emission are detected). The agreement between the atomistic and continuum results is generally good, except very close to the crack tip, where nonlinear effects as well as scattering of loading waves manifest themselves in the simulation. In figure 11, we use an extrapolation procedure to compute the stress intensity factor associated with this loading:

$$K_{\text{MD}} = \lim_{r \to 0} (2\pi r)^{1/2} S_{yy}(r) = 0.737 \,\text{MPa} \,\text{m}^{1/2}.$$
 (9)

This value of the stress intensity factor agrees well with the expected value

$$K_{\rm I} = \sigma_{\rm A} \sqrt{\pi \ell_0} = 0.793 \,\text{MPa} \,\text{m}^{1/2}.$$
 (10)

The atomistic results shown in figures 10 and 11 suggest that the parameters $K_{\rm I}$ and T provide an adequate description of the stress field and that their use in continuum predictions of the brittle–ductile behaviour leads to consistent cross-model comparisons. The T-stress profile near the crack tip obtained from the MD simulation (see figure 10) is typical of all biaxiality ratios α considered in this paper.

As seen in table 1, if T is near its maximum negative value considered here (at $\alpha=0$), the threshold for dislocation nucleation G_{disl} is smallest, in favour of ductile behaviour. If T increases towards zero (at $\alpha\approx1$), the likelihood of brittle crack initiation increases. Thus, there should exist some crossover value of α for brittle/ductile behaviour. To verify this, MD

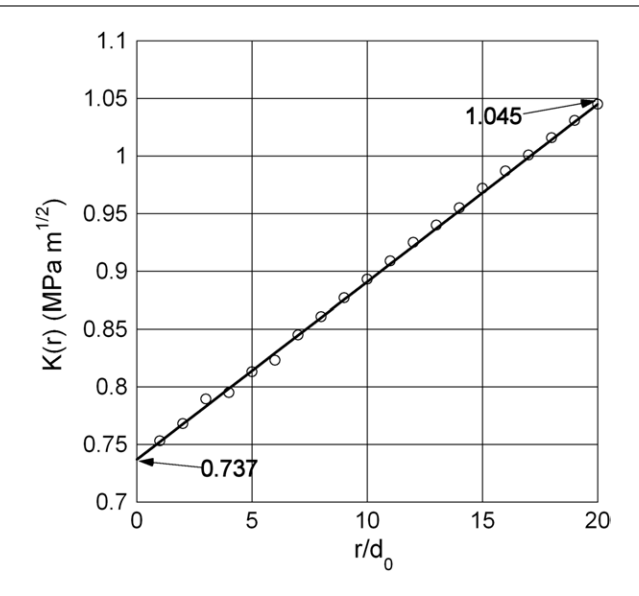


Figure 11. Linear extrapolation procedure for the stress intensity factor K_{MD} from the stress component S_{yy} in MD shown in figure 10 (sample size 300×432).

Table 2. MD simulation results under biaxial loading.	For this system.	, the Griffith level for fra	acture
is $K_G = 0.965 \text{MPA} \text{m}^{1/2}$.	•		

α	Process	Time step	$\sigma_{\rm a}$ (GPa)	$K_{\rm A}~({\rm MPa}{\rm m}^{1/2})$	T (GPa)
0.0	Symmetric dislocation nucleation	6667	7.58	0.88	-6.71
0.1	Symmetric dislocation nucleation	6760	7.68	0.89	-6.04
0.2	Symmetric dislocation nucleation	6863	7.80	0.91	-4.68
0.3	symmetric dislocation nucleation	6986	7.94	0.92	-4.65
0.4	Symmetric dislocation nucleation	7161	8.14	0.95	-3.95
0.5	Asymmetric dislocation nucleation	7280/7753	8.28/8.81	0.96/1.02	-3.19/-3.40
0.6	Asymmetric dislocation nucleation	7316/7777	8.32/8.84	0.97/1.03	-2.37/-2.56
0.7	Asymmetric dislocation nucleation	7272 / 7839	8.27/8.91	0.96/1.04	-1.54/-1.65
0.8	Bond breakage	6800	7.73	0.90	-0.66
0.9	Bond breakage	6794	7.72	0.92	+0.11
1.0	Crack initiation	7301	8.30	0.97	+0.95
1.1	Crack initiation	7287	8.28	0.96	+1.77
1.2	Crack extension	7261	8.25	0.96	+2.59

simulations under biaxial loading have been performed for several values of α , i.e. for different T values. The complete results are summarized in table 2.

For a biaxiality ratio $\alpha=1$ (that is, $T\approx0$), brittle crack initiation is observed in the simulations. The crack initiates at an applied stress intensity $K_{\rm A}\approx0.964\,{\rm MPa}\,{\rm m}^{1/2}$. The associated energy release rate at fracture initiation is $3.85\,{\rm J}\,{\rm m}^{-2}$, close to the theoretical work of decohesion $2\gamma_{\rm s}=3.603\,{\rm J}\,{\rm m}^{-2}$ (obtained in a perfect crystal strained axially in the $\langle 1\,1\,0\rangle$ directions under plane strain conditions). Using the anisotropic constant C discussed earlier, the theoretical Griffith stress intensity factor is $K_{\rm G}=0.965\,{\rm MPa}\,{\rm m}^{1/2}$, in good agreement with the MD results. For biaxiality ratios $\alpha=1.1$ and $\alpha=1.2$ (positive T-stress), cleavage crack extension (see figure 12) is observed at applied stress intensity factors of $K_{\rm A}=0.963$ and $K_{\rm A}=0.959\,{\rm MPa}\,{\rm m}^{1/2}$, respectively.

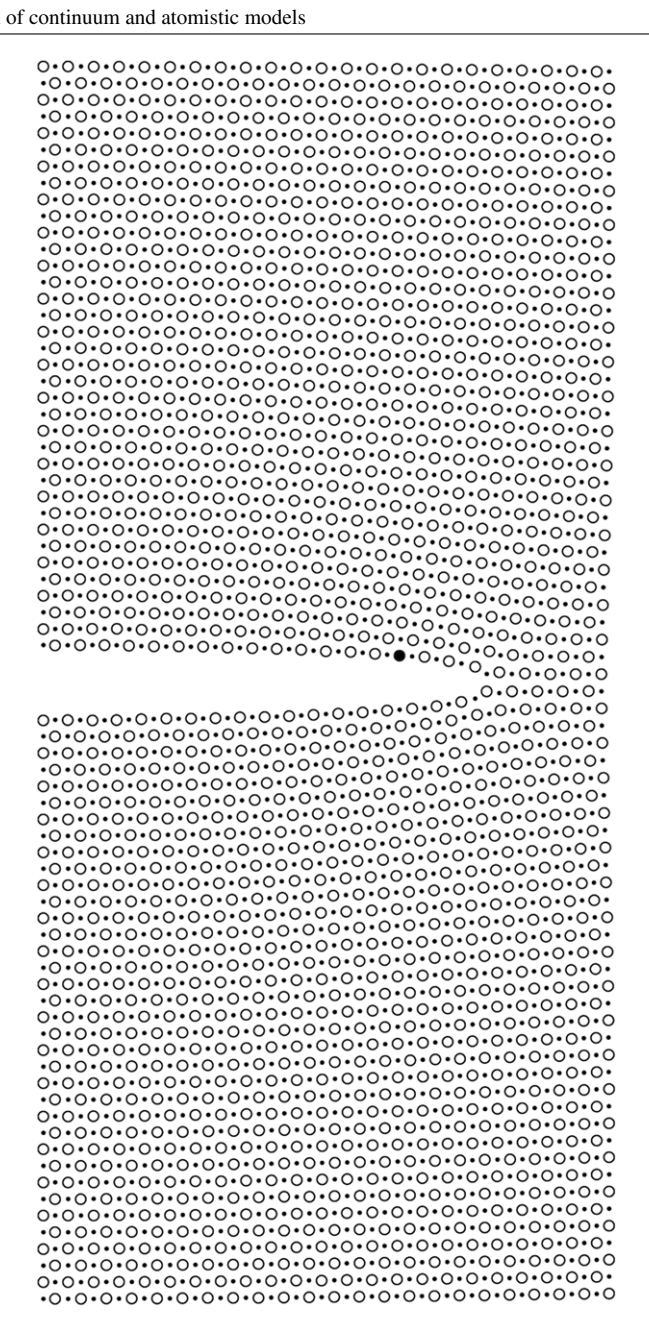


Figure 12. Brittle crack extension during linear loading for biaxiality ratio $\alpha = 1.2$ (time step 7450). The original crack tip atom is denoted in black (sample size 300×432).

For $\alpha = 0.9$ and $\alpha = 0.8$, significant bond breakage and crack tip opening are observed in the simulation, but full crack initiation does not occur prior to the arrival of stress waves emitted from the crack tip and reflected back from external sample borders to the crack tip (expected at time step \sim 8200). Nonetheless, the bond breakage is indicative of brittle behaviour.

For $\alpha = 0.7$, an 'asymmetric' dislocation emission from the crack tip is observed. The first complete dislocation is emitted on a slip plane $(111)\{112\}$ at the crack tip at time step

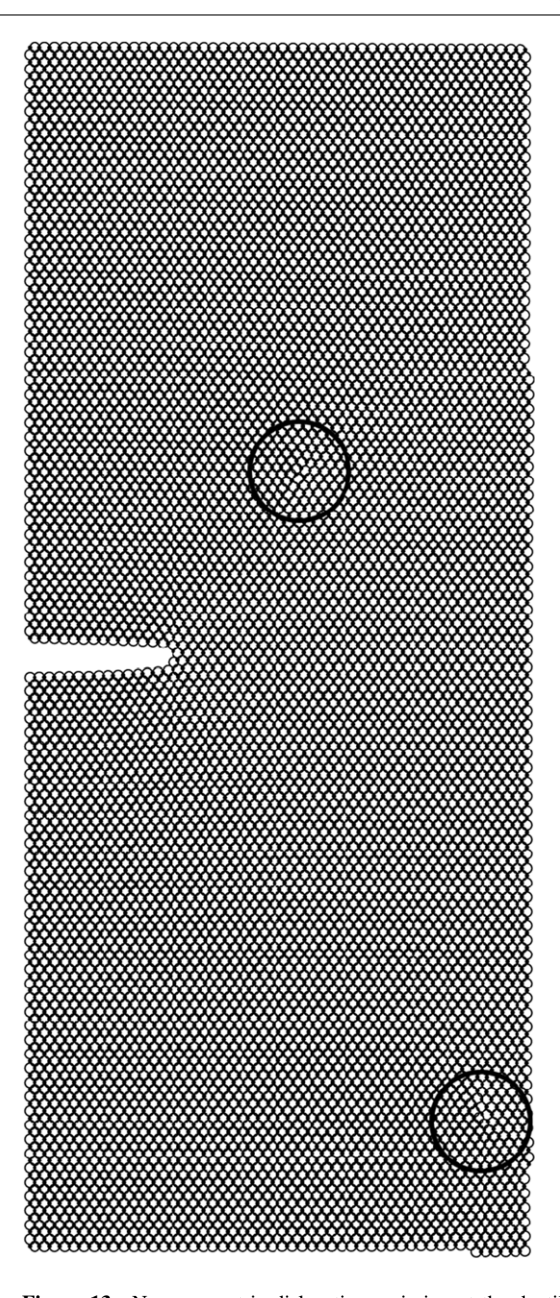


Figure 13. Non-symmetric dislocation emission at the ductile–brittle interface with biaxiality $\alpha = 0.6$ (time step 8000); sample size 300×432 .

7272. Emission of the second dislocation occurs on a slip plane $\langle 1\,1\,1\rangle\{1\,1\,2\}$ in front of the crack tip at time step 7839. These emission events correspond to applied stress intensities $K_{\rm A}=0.961$ and $1.036\,{\rm MPa\,m^{1/2}}$. Similar behaviour is observed for $\alpha=0.6$ (figure 13) and $\alpha=0.5$.

Symmetric dislocation emission at the crack tip occurs for $0 \le \alpha < 0.5$, as summarized in table 2. For the case $\alpha = 0$ (figure 14), we observe that dislocation emission occurs

Figure 14. Dislocation emission under linear loading at $\alpha = 0$ (time step 6668); sample size 300×432 .

at time step 6667, corresponding to an applied stress intensity $K_{\rm A}\approx 0.881\,{\rm MPa}\,{\rm m}^{1/2}$, in good agreement with the results presented earlier for uniaxial loading. As mentioned in the introduction, in the case of uniaxial loading ($\alpha=0$), the $(\bar{1}\,1\,0)[1\,1\,0]$ crack is much more stable than the $(0\,0\,1)[1\,1\,0]$ crack. This is in qualitative agreement with the simulations of Kohlhoff *et al* [29] and also with recent fracture experiments [30] performed under uniaxial loading on iron silicon (3 wt%) crystals of the same orientation. Extensive crack blunting and activation of the inclined $\langle 1\,1\,1\rangle\{1\,1\,2\}$ slip systems have been observed in the experiments with crack orientation $(\bar{1}\,1\,0)[1\,1\,0]$, similar to what is predicted here.

We note that the applied stress in the MD simulations is orders of magnitude higher than what is reported in experiments. This discrepancy can be understood in the framework of fracture mechanics: cleavage fracture or dislocation emission occur when the applied stress intensity factor K_A reaches the critical Griffith value K_G or $K_{\rm disl}$ needed for dislocation

emission, both considered as intrinsic material parameters. The applied stress needed for a given process to occur is then either $\sigma_A = K_G/(\pi l_0)^{1/2}$ or $\sigma_A = K_{disl}/(\pi l_0)^{1/2}$. Since the cracks in experiments are usually orders of magnitude longer, the applied stress needed for the processes mentioned above can be smaller. This geometric effect is expected to have no bearing on the main conclusions of this paper. Also, the three-dimensional aspect of dislocation nucleation is expected to manifest itself in experimental observations. Here, the emission of curved dislocations or loops is expected and, of course, thermal activation plays a role [31–33].

The continuum results in figure 2 show that a transition takes place for ductile to brittle behaviour for the $(\bar{1}\ 1\ 0)[1\ 1\ 0]$ crack as α increases through $\alpha=0.5$, where the horizontal line $2\gamma_s/\gamma_{us}=3.40$ (calculated from the data for the used potential given above) intersects the continuum curve G_{disl}/γ_{us} . This constitutes reasonable agreement with the MD results presented in table 2, where the transition region lies in the interval $0.5 < \alpha \le 0.7$.

5. Summary

The stress fields that develop near a crack tip in atomistic simulations of iron can be accurately characterized by a two-parameter asymptotic field using the stress intensity factor $K_{\rm I}$ and the T-stress. This supports our use of $K_{\rm I}$ and T in continuum predictions for ductile versus brittle behaviour.

Our continuum and atomistic modelling of bcc iron suggests that the T-stress plays a significant role in determining the ductile versus brittle response of a crack tip and plays a role in the crack size effect. Specifically, the reasonable agreement that we find is especially relevant for small cracks, for which the T-stress, if it is neglected, can cause significant disagreement between the continuum and atomistic predictions.

Acknowledgments

The work was supported by the National Science foundation (USA) under grant CMS-0000142 and by the Grant Agencies of the Czech Republic under grants A2076201 (Czech Academy of Sciences), ME 504 (Czech Ministry of Education) and AV0Z20760514. CEB would like to acknowledge invaluable discussions with Alexei E Romanov.

References

- [1] Mullins M and Dokainish M A 1982 Phil. Mag. A 46 771
- [2] Dienes G J and Paskin A 1987 J. Phys. Chem. Solids 40 1015
- [3] Shastry V and Farkas D 1996 Modelling Simul. Mater. Sci. Eng. 4 473
- [4] Cleri F, Yip S, Wolf D and Phillpot S R 1997 Phys. Rev. Lett. 79 1309
- [5] Rice J R 1992 J. Mech. Phys. Solids 46 239
- [6] da Silva K D, Beltz G E and Machová A 2003 Scr. Mater. 49 1163
- [7] Beltz G E and Machová A 2004 Scr. Mater. 50 483
- [8] Beltz G E and Fischer L L 2001 Multiscale Deformation and Fracture in Materials and Structures ed T J Chuang and J W Rudnicki (Boston: Kluwer) pp 237–42
- [9] Sun Y, Beltz G E and Rice J R 1993 Mater. Sci. Eng. A 170 67
- [10] Machová A, Beltz G E and Chang M 1999 Modelling Simul. Mater. Sci. Eng. 7 949
- [11] Machová A and Ackland G J 1998 Modelling Simul. Mater. Sci. Eng. 6 521
- [12] Landa M, Cerv J, Machová A and Rosecký Z 2002 J. Acoust. Emiss. 20 25
- [13] Nielsen O H and Martin R M 1985 Phys. Rev. B 32 3780
- [14] Cheung K S and Yip S 1991 J. Appl. Phys. 70 5688
- [15] Machová A 2001 Modelling Simul. Mater. Sci. Eng. 9 327
- [16] Sih G C and Liebowitz H 1968 Fracture vol 2 ed H Liebowitz (New York: Academic) pp 67–190

- [17] Savin G N 1961 Stress Concentration Around Holes (New York: Pergamon)
- [18] Stroh A N 1958 Phil. Mag. 7 625
- [19] Rice J R 1974 J. Mech. Phys. Solids 22 17
- [20] Sun Y and Beltz G E 1994 J. Mech. Phys. Solids 42 1905
- [21] Frenkel J 1926 Z. Physik. 37 572
- [22] Beltz G E 1992 The mechanics of dislocation nucleation at a crack tip PhD Dissertation Harvard University Cambridge, USA
- [23] Beltz G E and Rice J R 1992 Acta Metall. Mater. 40 S321
- [24] Hearmon R F S 1961 Introduction to Applied Anisotropic Elasticity (Oxford: Clarendon)
- [25] Paidar V 1983 Phil. Mag. A 52 73
- [26] Vitek V 1970 Scr. Metall. 4 725
- [27] Murakami Y 1987 Stress Intensity Factor Handbook vol 1 (Oxford: Pergamon)
- [28] Fett T 1998 A compendium of T-stress solutions Research report FZKA 6057 Forschungszentrum Karlsruhe GmbH
- [29] Kohlhoff S, Gumbsch P and Fischmeister H F 1991 Phil. Mag. A 64 851
- [30] Spielmannová A, Landa M, Machová A, Haušild P and Lejček P 2006 Influence of crack orientation on the ductile-brittle behavior in Fe-3wt%Si single crystals *Mater. Charact.* at press
- [31] Schoeck G and Puschl W 1991 Phil. Mag. A 64 931
- [32] Schoeck G 1991 Phil. Mag. A 63 111
- [33] Rice J R and Beltz G E 1994 J. Mech. Phys. Solids 42 333